XBEX: X-ray Background EXplorer

A next-generation hard x-ray survey telescope proposal

T. Harvey (29974232)

April 2020

1 Executive Summary

XBEX is a hard x-ray all-sky survey mission that will be sensitive across the 10-300keV range for imaging and spectroscopy. It will primarily investigate the x-ray background, with the mission of resolving many more of the individual sources that contribute to its non-stellar continuum. XBEX will catalogue an order of magnitude more AGN, including Compton-thick AGN, than it's predecessors, including the Swift and INTEGRAL telescopes. In their all-sky surveys, Swift has observed around 1600 hard x-ray sources (Oh et al., 2018) and INTEGRAL has discovered around ~1000 emitting objects (Bird et al., 2016), whereas XBEX is expected to catalogue over 10,000 extragalactic sources during its 3 year survey, including between 700 and 2000 new Compton-thick AGN. XBEX has 4x times better continuum sensitivity than INTEGRAL or Swift across its energy range.

XBEX will conduct the most unbiased survey of the deep extragalactic sky, and will identify many more Compton-thick AGN at intermediate redshift, allowing investigation of the true proportion of AGN that are Compton-thick, and whether this proportion changes with redshift, which would have a large impact on theories of AGN evolution and the link between AGN and their galaxies. XBEX will also watch for new transient sources, and allow us to more accurately study new classes of object, such as x-ray bright optically normal galaxies (XBONGS). The science payload consists of a coded mask telescope, using a square twin-prime uniformly redundant array (URA), which has the benefit of having a delta-function for its point spread function, rather than the noisy sidelobes associated with a random mask. The detector is comprised of 4445 1.5 x 1.5 x 1cm CZT crystals, each of which is subdivided into 225 "virtual" 0.1 x 0.1 cm pixels, which will make XBEX the first megapixel hard x-ray telescope with a total detector area of $10,000 cm^2$. This massive step up in the number of detector crystals is due to recent advances in the growth of CZT crystals, and the development of very power-efficient readout electronics. The use of a large number of small pixels makes it possible to have a large detector area, which allows for good sensitivity, while the small pixel size means the detector has high spatial resolution, which means this telescope has a much better angular resolution and point source location accuracy than its predecessors. XBEX will have an angular resolution of 3.4', and a PSLA of 14". The half coded field of view of the telescope will be ~36°by ~36°, and the telescope will observe the whole sky every ~48 hours.

The mission will also have a secondary payload of a soft x-ray telescope, which will perform complimentary observations in the 0.5 - 10 keV energy band, including characterising the the column density of the AGN observed in the hard x-ray band, and observing the 6.4keV fluorescent iron line, which is another indicator of obscured AGN.

XBEX will launch in late 2027 on an Ariane 6.2 mission from Kourou, French Guiana, as part of a ridesharing mission, and will go into an low equatorial (i= 0°) orbit at around 600km. This orbit will afford the spacecraft protection from some cosmic rays by being inside the Earth's magnetic field, while also being high enough to remain in orbit for its nominal 5 year mission without excessive orbital decay and mostly avoid the South Atlantic Anomaly (SAA). The science payload has a mass of ~3560kg. The 5 year mission will consist of a 3 year all-sky survey, and 2 years of specific pointings and time for guest observers.

2 Introduction

The first studies of x-ray and γ-ray sources only began in the 1960s, since the upper atmosphere absorbs incident high energy photons. Observational high energy astronomy only really began during the space-race, when it became possible to send useful payloads out of Earth's atmosphere. The first observation of a non-stellar x-ray source was from a Aerobee 150 rocket launched in 1962, which detected x-rays from Scorpius X-1 (Giacconi, 2003). Since then numerous missions, some on satellites, and some carried by balloon, have answered many questions about the nature of the high energy sources we observe.

These high energy sources include active galactic nuclei (AGN), which are some of the most luminous and distant non-stellar sources ever observed, gamma-ray bursts, which are random, brief bursts of high energy radiation, and x-ray binaries, which are binary pairs of a compact object(White dwarf, neutron star or black hole) and a main sequence star (Frank et al., 2002). Many examples of these objects have been observed by a succession of all-sky survey missions, and the current high energy survey missions include the INTErnational Gamma-Ray Astrophysics Laboratory (INTEGRAL) and the Neil Gehrels Swift Observatory (known as Swift). INTEGRAL was launched in 2002, and Swift in 2004, meaning that both satellites were designed in the 1990s, over 20 years ago. They have both operated for over 15 years, well beyond their original mission lifetime, and continue to operate to this day, which is a testament to their design. INTEGRAL will re-enter the Earth's atmosphere and burn up in 2029 ESA (2015), and there is no guarantee how much longer Swift will continue to be operational for, so in this paper I propose a new, replacement hard x-ray all-sky survey telescope. This mission, named the X-ray Background EXplorer, or XBEX, will launch in the late 2020s and will be based on similar principles to it's predecessors, but modernised and applied on a much larger scale. This will allow for both improved sensitivity and source location, and will enable us to answer some of the biggest questions in high energy astrophysics.

This mission would be complementary to other current and proposed missions, such as the Nuclear Spectroscopic Telescope Array (NuSTAR) satellite, which operates between 3 and 79keV, and the Advanced Telescope for High Energy Astrophysics (ATHENA) mission, which is currently in development and will operate between 0.2 - 12 keV (Barcons et al., 2015). These telescopes, and XBEX, will operate in different but overlapping energy bands, so research will be able to be carried out using observations from all 3 missions, over a greater energy range than any individual mission.

3 Science Aims and Background

In this section I will go over some of the types of x-ray sources we observe, both galactic and extragalactic, highlight some of the big questions that still need answering, and give an overview of the current hard x-ray missions. I will state and explain a number of science goals for XBEX, and furthermore I will lay out a set of technical requirements for XBEX, if it is to successfully meet these goals.

3.1 Accretion and Galactic X-Ray Sources

The majority of x-ray sources, with the exception of some sources in the galactic centre, are powered by accretion. Accretion is the process by which matter infalling onto a massive object releases its gravitational potential energy in the form of electromagnetic radiation (see Frank et al., 2002). Accreting sources can be split into 2 categories, those that are galactic and those that are extragalactic. The galactic sources that emit at wavelengths we are interested in (>10 keV) tend to be x-ray binaries, which can be split into high mass x-ray binaries (HMXBs) and low mass x-ray binaries (LMXBs). X-Ray binaries are defined as a compact objects, such as white dwarfs, neutron stars or black holes, orbiting in a binary system with a stellar mass companion star. The x-ray binaries accrete matter from the companion by Roche-lobe overflow (Paczynski, 1971) through the L1 point of the system. Conservation of angular momentum means this material will form an accretion disc, as it slowly spirals into the gravitational well of the primary object. Friction in this disc causes high temperatures that can be in excess of 1 million °K, and which therefore emits in x-rays (Frank et al., 2002). The difference between LMXBs and 'HMXBs is the mass of the companion star, in LMXBs the star is of or below category A in the MK system, or sometimes a white dwarf with a mass

below $2M_{\odot}$. The companion star is generally completely outshon by the primary. A HMXB has a O/B type companion star with an optical luminosity on the same order of magnitude as the x-ray source (A. Bird, 2020).

3.2 Extragalactic Sources

Extragalactic sources are principally AGNs which consist of Quasi-Stellar Objects (Quasars), Seyfert galaxies and BL-Lac objects. You can also get radio-loud and radio-quiet versions of each source depending on which band they have a higher emission in. Seyfert galaxies have quasar-like centres, but with a clearly detectable host galaxy. They can be split into two categories, type I and type II, depending on the presence of broad and narrow emission lines in their spectra. Seyfert I galaxies have narrow (several hundred km/s) forbidden and permitted lines, and only permitted broad (up to 10^4 km/s) lines, whereas Seyfert II galaxies only have narrow lines. (Peterson, 1997). Quasars are similar to Seyfert galaxies, but are much more luminous and at high redshift (z > 0.1). Their host galaxies are much dimmer than the central object so they appear as point sources.

BL-Lac objects are comparable to QSO's, but vary on much shorter timescales and at all wavelengths. They also have a highly polarised optical continuum and no emission lines (Aleksić et al., 2012). Most AGNs can be described by a single unified model, which consists of of a super-massive black hole with a hot accretion disk which emits from optical to x-ray. The disk is surrounded by orbiting gas, the closer of which is referred to as a broad line region (BLR) due to the high orbital velocity of the gas and the subsequent Doppler broadening of its emission lines. The gas which orbits at a greater distance is called the narrow line region (NLR) as it has a lower velocity and hence narrow spectral lines. This whole system can be obscured by a dusty torus when viewed edge-on, which generally emits in IR (Symeonidis et al., 2016). The AGN can also have jets extending from the poles which can propel matter at high velocities for hundreds of kilo-parsecs. These jets are often known as radio jets because they can emit strongly in radio waves. The classification we give an AGN depends on the viewing angle relative to the observer, and many, but not all, of the different types of AGN observed are thought to be similar objects seen from different angles (Antonucci, 1993).

We can also more generally refer to type I and II AGN depending on whether the nucleus is obscured; type I AGN emit both broad and narrow lines whereas type II AGN only emit narrow lines. This may be because of viewing angle or a structural difference (Ramos Almeida, 2011). An obscured AGN is defined as one with a column density N_H greater than $10^{22} cm^{-2}$, as defined in Malizia et al., 2012 and references therein, because it is high enough to obscure the broad line region. We also define Compton-thick as $N_H \geqslant 1.5 \times 10^{24} cm^{-2}$, as is done in the previous source. This value is defined as Compton thick as it is the inverse of the Thompson-cross section (σ_T^{-1}), which is the optical depth of 1 for Compton-scattering. Current surveys have a bias against detecting high redshift Compton-thick AGN. The larger the value of N_H and the worse the sensitivity of the survey, the more the survey is biased towards unabsorbed sources. Malizia et al., 2012 finds that 7% of AGN are Compton-thick without accounting for this bias, and 20-24% when the bias is accounted for using a low redshift cutoff of z < 0.0015.

AGN also emit in the Mid-IR, which is produced by emission by the toroidal dust, heated by the continuum emission from the SMBH (see García-Burillo et al., 2016). The IR emission of an AGN is characteristic and is commonly used to identify AGN without needing to observe them in hard x-ray. The mid-IR emission is fitted to a power law with a different slopes for Type 1 and Type 2 AGN. The ratio of emission in different IR bands, called WISE colours, has been used to identify some low redshift AGN, (see Stern et al., 2012, Kilerci-Eser et al., 2020) however as detailed below, newer research suggests that WISE identification only works in some cases. It is also often impossible to match an object observed in IR with a telescope such as Spitzer, which can often pinpoint sources <1", to a hard x-ray source as the source location accuracy of hard x-ray telescopes is often several orders of magnitude worse, meaning that you get source confusion where you can't be sure which source is emitting. The next-generation telescope proposed here would have a much better source location accuracy than telescopes like Swift-BAT or INTEGRAL, and would allow for much easier mid-IR observation of observed hard x-ray sources and vice versa.

The absorption distribution among the different types of AGN and the overall proportion of absorption is an important question in the study of AGN. According to Gilli et al., 2007, modelling the cosmic x-ray

background as a combination of absorbed and unabsorbed AGN has been successful in reproducing the observed background, but it requires knowledge of the absorption of AGN. At energies >15 keV only ∼1% of the CXB can be resolved into point-like sources, whereas in soft x-ray nearly 100% of the CXB can be resolved into discrete objects (Bottacini and Ajello, 2012). These objects, often identified in deep surveys by Chanda or XMM-Newton, show that a large proportion of them are obscured Type 2 AGN at around $z \sim 1$ (Barger et al., 2005, Brusa et al., 2010). There are also many questions still to be answered about obscured AGN, such as the number of type 2 QSOs and about the nature of a recently discovered class of object called X-ray Bright Optically Normal Galaxies (XBONGs). XBONGs are optically dull, but have a high x-ray luminosity of $10^{43} - 10^{44}$ erg s^{-1}. Several theories have been proposed to explain this, including heavy uniform obscuration of the AGN, and the dilution of nuclear emission by starlight, but there is a very limited sample size of these objects, and a more sensitive survey, that identified more objects would be necessary to explain their unusual properties (Malizia et al., 2012). According to Malizia et al., 2012 and Oh et al., 2018, photons transmitted from Compton-thick AGN are absorbed between 2-10 keV, hard x-ray photons above 10 keV can pass through the gas and dust obscuring even Compton-thick sources. Results from Koss et al., 2016 suggest that surveys above 10keV may be the only way to consistently identify such Compton-thick AGN, as other methods, such as $F_{OIII} : F^{obs}_{2-10keV}$ and WISE colours, only correctly identify a minority of Compton-thick AGN. The authors further suggest that a higher fraction of nearby AGN may be Compton-thick, and estimate a percentage of 22% in the local Universe, which is a conservative estimate due to the bias of their data-set against absorbed AGN. This is contrary to previous estimates of the fraction of AGN that are Compton-thick, such as the 9% suggested in Vasudevan et al., 2013. A higher percentage would be in line with the estimates of Compton-thick AGN needed to reproduce the observed x-ray background (e.g. Ueda et al., 2014).

Some bright, high redshift (z > 1) Compton-thick AGN can be studied using the 0.5-10keV observatories, such as XMM-Newton or Chandra, as the >10keV emission has red-shifted into the region accessible to these telescopes (see Lanzuisi, G. et al., 2015). However, less luminous and lower redshift sources are not accessible using these methods, and require direct observation in the relevant wavebands. It is often useful to combine source observations in different wavebands, as observations to determine column density of N_H are much easier below 10keV as soft x-ray emission is more dependent on absorption than hard x-ray emission (see Gilli et al., 2007).

As discussed above, AGN obscuration is thought to be due to a large gas and dust torus surrounding the AGN. Many other studies have been done on modelling these tori using Monte Carlo simulations, such as Furui et al., 2016, Liu and Li, 2014 and Baloković et al., 2018. Some of the newer models leave the torus geometry as a free parameter, which allows us to learn a lot about constrains on these obscuring tori. However these models are generally very complex, and the use of them requires high quality hard x-ray spectra up to around 100 keV. According to A. Bird, 2020, 40% of AGN hard x-ray emissions are variable on timescales of less than one day, and 97% are variable, over periods of weeks to months. The variability of AGN is an important tool for estimating the size and mass of the AGN using a travel-time argument. This limits the size of the AGN by saying that the AGN can't vary on timescales shorter than required for light to travel across it, and using the speed of light we can determine an upper limit on the size (R) of the AGN using $R < c\delta t$, where δt is the shortest variability of the emission and c is the speed of light.

3.3 Extragalactic Log N - Log S Distributions

A wide variety of x-ray sources have been identified and studied in detail. There are merits to highly detailed observational studies of single x-ray sources, which can teach us a lot about the processes inside such a highly energetic system, but to fully understand these objects we need a statistical study which looks at a large number of sources. Such studies have been made by a variety of groups, most notably in the last 20 years by the INTEGRAL and SWIFT observatories. With a large statistical sample we can construct an X-ray Luminosity Function (XLF) for AGN sources, as well as hard x-ray source number densities (log N - log S). Current log N - log S plots allow us to estimate how many new sources a more sensitive next-generation hard x-ray telescope would detect. Log N - log S distributions for hard x-ray sources can be found in Bottacini et al., 2012, Ajello et al., 2012, Akylas and Georgantopoulos, 2019 and Mateos, S. et al., 2008, and the fits from a few of the relevant ones are displayed in Figure 1, along with the equations of the

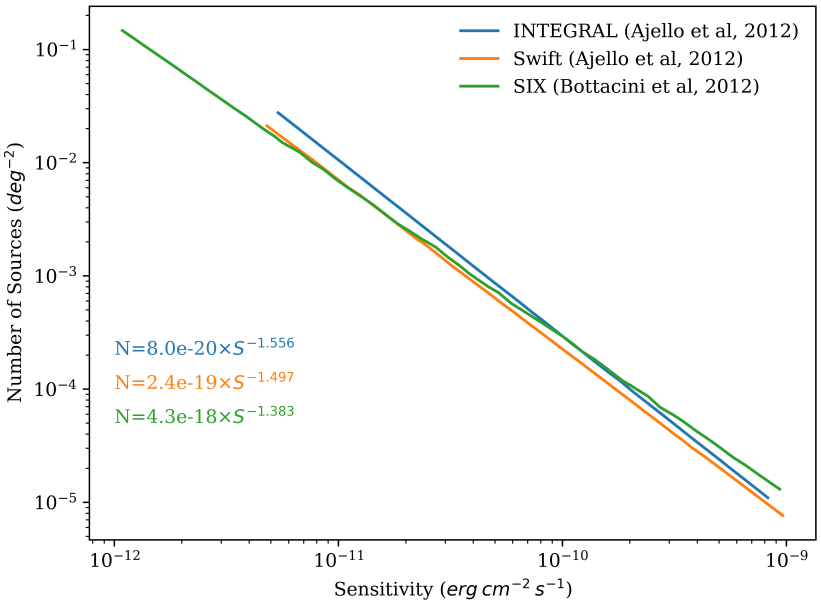

Figure 1: Graph showing the fits of the integrated number count for AGN, derived from measurements from the Integral (Bottacini and Ajello, 2012, blue), Swift (Ajello et al., 2012, yellow), and SIX (Bottacini et al., 2012, green) surveys, along with the corresponding equation of power-law fit for each.

power-law relation for each one. The fit of the Log N - log S plots is typically given as $N(>S) = K \times S^{\alpha}$ where $N(>S)$ is number of sources above the flux S, K is a normalisation constant and α is the exponent. Figure 1 shows the Log N - Log S figure from the SIX survey (18-55keV) (taken from Bottacini et al., 2012, see below) and the best fit is given by $\alpha = 1.38$, whereas the fit from the Swift data shown in Figure 1 (taken from Ajello et al., 2012) gives a value for α of $1.49^{+0.08}_{-0.07}$. The two values of α don't agree completely but they allow us to estimate how many more sources a more sensitive survey could detect, within a reasonable margin of error. One explanation for the difference in α and K values between surveys is the different hard x-ray bands the surveys (Swift-BAT (15-55keV), Integral(17-60keV), Nu-Star(8-24keV)) are conducted in, and the differing sensitivities and observing patterns of the surveys. There are many other calculations of Log N - log S distributions for hard x-ray sources, such as Akylas and Georgantopoulos, 2019, Krivonos, R. et al., 2007, and Treister et al., 2009. Fluxes can be converted between different bands using a power law with a given photon index.

Results from population synthesis models (see Treister et al., 2009, Draper and Ballantyne, 2010) and the 2-10keV band (see Xue et al., 2011, Rosati et al., 2002) suggest we can expect the slope of the log N - log S graph to be euclidean down to $\sim 10^{-14} erg\ s^{-1}\ cm^{-2}$ - around 50× as sensitive as the Swift-BAT survey. This means we can linearly extrapolate the slope of the log N - log S slope down to lower fluxes. The Log N - Log S relations shown in 1 can be used for this purpose. The number of sources per square degree at a given sensitivity can be multiplied by the number of square degrees in the sky ($\sim 41253\ deg^2$) to get the total number of sources detected.

Considering the number counts of only Compton-thick AGN has quite a bit more uncertainty than that of all AGN; not enough sources have been identified to conclude which of several models are correct. The model from Draper and Ballantyne, 2010, which suggests Compton-thick sources are a combination of low z, low Eddington ratio objects and high-z, high Eddington ratio, quasar-like objects, is different to other models where the proportion of Compton-thick AGN is a constant fraction of the AGN population. This leads to differences in the number of proposed Compton-thick AGN, for example the model of Draper and Ballantyne, 2010 predicts twice as many Compton-thick sources (with a 10-30keV flux $> 10^{-13}\ erg\ s^{-1}\ cm^{-2}$ at z<0.5) than the model from Franca et al., 2005. The number densities derived from these models, both for all AGN and only Compton-Thick AGN, are shown in Figure 2. The different models

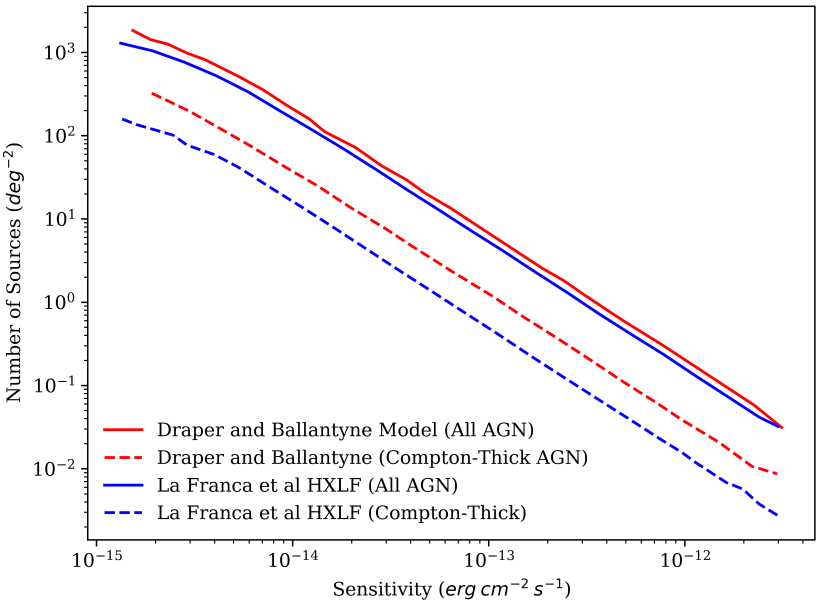

Figure 2: Solid lines show the integrated number count for all AGN, and dashed lines show the contribution from Compton-Thick AGN, for two different models. The blue lines show data taken from Franca et al., 2005, and the red lines show data taken from Draper and Ballantyne, 2010. Both are in the energy band 30-60keV, and for sources $0< z <5$.

can be tested by observing the slope at bright fluxes; the weakly accreting, low z objects in the Draper and Ballantyne, 2010 model cause a shallower slope than the fixed ratio model, due to the low luminosity of those AGN. This means determination of Compton-thick AGN count rate at z>1 and with good sensitivity ($\sim 10^{-13}\ erg\ cm^{-2}\ s^{-1}$) will allow measurement of the evolution of Compton thick AGN, and determine the relation, if any, to redshift. If the proportion of Compton thick AGN is higher at higher redshifts would have ramifications for our understanding of the link between AGN and galaxies (see Ballantyne et al., 2011).

Given the predicted sensitivity of XBEX, given in section 6.1, and the spectra of a canonical AGN ($\Gamma =\sim 1.7$), we can predict how many sources will be detected in a 3 year survey. The limiting sensitivity of the 3 year survey is predicted to be around $9 \times 10^{-13}\ erg\ cm^{-2}\ s^{-1}$ in the 10-100keV band. This limiting sensitivity was derived by integrating the differential sensitivity of the telescope (in $ph\ cm^{-2}\ s^{-1}\ keV^{-1}$), between 10 and 100keV, and converting from a photon flux to an energy flux considering a photon energy distribution from the SED of the canonical AGN in that energy band. Then using the log N - Log S plots given in figure 1, the number of extragalactic sources that will be observed is predicted to be $\sim 10,000$. This includes at least 700 Compton-thick (type 2) AGN, going by the model from Franca et al., 2005, or up to 2000, from the model from Draper and Ballantyne, 2010, both of which are shown in Figure 2, and can be fitted to power laws (at the limiting flux of this survey) and used to find the total number of objects in a similar way to above. The total number of AGN at our limiting sensitivity from both models also agree with the result derived above, and produce estimates of 9000-11000 total AGN. This is at least an order of magnitude more Compton-thick AGN than have been detected so far, most notably by the Swift and INTEGRAL surveys (Bird et al., 2016, Oh et al., 2018).

There are many other benefits to hard x-ray surveys (>15 keV). Firstly, the Compton-reflection bump, produced by reflection of radiation on the inside of the obscuring gas torus, peaks at 20-30keV (see Gilli et al., 2007. Secondly, this component dominates in nearby obscured AGN (Comastri et al., 2007), and also contributes directly to the shape and intensity the cosmic x-ray background which peaks at ~30keV and extends up to 50keV (see Türler et al., 2010, Ueda et al., 2003). The majority of accretion generated energy density in the Universe takes place in obscured AGN (see Fabian et al., 1998), which makes understanding these objects critical to understanding the history and evolution of AGN.

3.4 Previous Missions

Over the past 20 years great advances in hard x-ray (10 - 250 keV) surveys have been made by the IBIS detector on the INTEGRAL observatory and by the Burst Alert Telescope (BAT) on the SWIFT observatory. Since it launched it 2002 INTEGRAL has located 939 objects, over a 4.5σ detection threshold, in the 17-100keV range across the whole sky (Bird et al., 2016). However most of these detections are biased towards the galactic plane and indeed a separate galactic plane ($|b| < 17.5°$) catalog is available at Krivonos et al., 2012 which lists 402 objects over a 4.2σ threshold. As the IBIS detector has a point source location accuracy of 0.5' - 4', the high source density in the galactic core region ($4° \times 2°$) means that there are many unresolved sources, and many sources that are below the detection threshold, meaning there is a non-uniform background and much higher levels of systematic noise. This means the INTEGRAL survey has to be very conservative in the galactic core region, as per Bird et al., 2016 .The low energy array on IBIS is called ISGRI, and is a pixelated Cadmium Telluride (CdTe) detector that works between 17-1000 keV. According to Krivonos et al., 2012 the INTEGRAL galactic plane survey covered 90% of the galactic plane to a sensitivity of $2 \times 10^{-11} erg\ s^{-1}\ cm^{-2}$ and 10% to a sensitivity of $4.9 \times 10^{-12} erg\ s^{-1}\ cm^{-2}$.

The Swift-BAT mission has also conducted a more uniform all-sky survey with a sensitivity of $8.4 \times 10^{-12} erg\ s^{-1}\ cm^{-2}$ over 90% of the sky and $7.24 \times 10^{-12} erg\ s^{-1}\ cm^{-2}$ in the 14 - 195 keV band according to Oh et al., 2018. The authors detected 1632 objects above 4.8σ, including 448 Seyfert II's (27.5%), 379 Seyfert I's (23.2%), 148 Beamed AGN/Blazars (9.1%), 114 unknown AGN (7%), 109 LMXBs (6.7%) and 108 LMXBs (6.7%). Swift-BAT is more successful at identifying absorbed AGN due to its use of the 14-195keV band however it is still biased against the most absorbed AGN with $N_H > 10^{25} cm^{-2}$ (Koss et al., 2016).

The INTEGRAL (Bird et al., 2016) and Swift-BAT (Oh et al., 2018) surveys are complimentary, as the INTEGRAL mission has a better angular resolution ($\sim$ 12' of FWHM vs 19.5' for SWIFT) but is more concentrated in the galactic plane, whereas SWIFT has a considerably higher average exposure time over the extragalactic sky. Swift points close to randomly, whereas INTEGRAL performs specific observations and exposures mainly along the galactic plane. This means Swift-BAT detects more extragalactic sources, such as AGNs. (see Oh et al., 2018). When a similar exposure time on the extragalactic sky is compared, the Swift-BAT sample contains ~70% extragalactic sources (Cusumano et al., 2010) whereas the INTEGRAL sample contains around 35% (Bird et al., 2016).

A 'virtual' mission combining data from Swift and Integral known as Swift-INTEGRAL X-ray (SIX) survey was performed (see Bottacini et al., 2012, Bottacini and Ajello, 2012), which looked at 6200 deg^2 of sky at 18-55keV with a limiting flux of $\sim 3.3 \times 10^{-12} erg\ s^{-1}\ cm^{-2}$, which is more sensitive than either individual survey. This survey was very successful in eliminating the statistical noise from the individual surveys, which is a common problem with coded-mask telescopes (see Skinner, 2008). Coded-mask telescopes are often used for surveys because of their good sensitivity in a wide energy band (up to 1MeV) and large field of view. However they suffer from poor sensitivity due to the lack of focusing optics and the fact that by design ~50% of the incoming photons are blocked by the mask. Some other modern generation telescopes, such as NuSTAR, employ focusing optics to observe hard x-rays. NuSTAR uses coated grazing-incidence mirrors and an extended detector to achieve a focal length of 10m and a energy range of 3-79keV. Incoming x-ray photons must have a a very low angle of incidence to the mirrors to reflect and not pass straight through, so very large focal lengths are needed, meaning such telescopes have to be very long (A. Bird, 2020). NuSTAR has a very good sensitivity in its energy range, but is not suited to conducting an all-sky survey as it has a small field of view (12' x 12'), conducts its survey in very specific areas of the sky, and furthermore has a limited energy range due to the nature of its focusing optics.

The telescope proposed here would allow us to determine the nature of the x-ray background above 20keV, and to resolve many more of the faint x-ray sources than make up the x-ray background. XBEX will also allow us to learn much more about Type 2 AGN, and will be able to determine the proportion of Type 2 AGN in the local universe, including the investigation of unusual objects such as XBONGs. As discussed above, gathering high quality x-ray spectra up to 100keV is also important for testing Monte Carlo models of AGN obscuration. A larger sample size of obscured AGN will also allow us to derive their x-ray luminosity function, and a much larger sample of Compton-thick AGN will allow the determination of the dependence of the number density of these objects, and their redshift. The number of extragalactic sources that will be

observed in 3 years of observations, worked out from the above log N - log S fits and the sensitivity of the XBEX telescope given in 6.1, was estimated to be 10,000 at a limiting flux of $\sim 9 \times 10^{-13}\ erg\ s^{-1}\ cm^{-2}$, This is an order of magnitude more sources than have currently been observed with Swift or INTEGRAL. The telescope will also watch the whole sky for new transient sources, including AGN.

3.5 Mission Requirements

To fulfill the science aims set out above there is a set of requirements that the telescope design needs to meet.

1. Look at the whole sky as often as possible, ideally every day. For an all-sky survey, the larger the field of view, the more time each individual "section" of the sky can be observed. This is important because many AGN are variable on the order of a day, and because one of the secondary science goals is to observe new transient sources, the likelihood of which is improved the more often the telescope observes each area of sky.

2. A sensitivity of $> 1 \times 10^{-12}\ erg\ s^{-1}\ cm^{-2}$ at hard x-rays of 10-300keV over the whole sky.

3. An angular resolution < 5', to be able to separate the $\sim$ 10,000 sources we expect to observe at these sensitivities. However angular resolution is secondary to point source location accuracy, as extragalactic objects tend to be spread more evenly over the sky, and hence more spaced apart from each other on average.

4. A point source location accuracy (PSLA) for a 5σ source of <30", to be able to match a hard x-ray source to a source in other bands, such as soft x-ray and IR.

5. A reasonable spectral resolution of <10% at 50keV, as spectral resolution, while important, is not one of the critical parameters for these observations.

6. A secondary payload soft x-ray telescope, sensitive between 0.5 and 10 keV, to allow for simultaneous observation across a wider energy band, and to allow for more accurate determination of the N_H column density to identify obscured sources.

4 Science Payload

XBEX showcases the next generation of hard x-ray telescopes. INTEGRAL and Swift were both designed over 20 years ago, and in that time technology and manufacturing processes have moved on at a rapid pace. This design employs similar technology as the INTEGRAL and Swift missions, but at a scale once thought impossible. Advances in semiconductor crystal growth techniques and power-efficient readout electronics have allowed XBEX to use larger detectors, and more pixels, than any other hard x-ray telescope operating in the same energy range.

Figure 3 shows the basic design for the science payload and spacecraft. The size of the mask, detector and the distance between them are too scale, but the rest of the spacecraft and the solar arrays are an estimate of the required size. The pattern shown for the mask is only meant as a representation, and is not the actual mask pattern that will be used.

4.1 Detector System

The detector will be comprised of 4445 pixelated Cadmium Zinc Telluride (CZT) crystals, with each pixel being 0.1 x 0.1 cm and the crystals each being 1.5 x 1.5 x 1cm. This allows for 225 'virtual' pixels per crystal. There will be 4445 closely-tiled pixelated crystals for a total of 1 megapixel and a total sensitive area of 10,000 cm^2. The use of 1cm thick CZT pixels means that XBEX will be sensitive to an unprecedented range of energy, with 50% of 400keV photons interacting in the detector. This represents a step up from the 32,000 4x4mm non-pixelated CZT crystals (total area $5200cm^2$ used in the Swift-BAT mission (see Barthelmy et al., 2005).

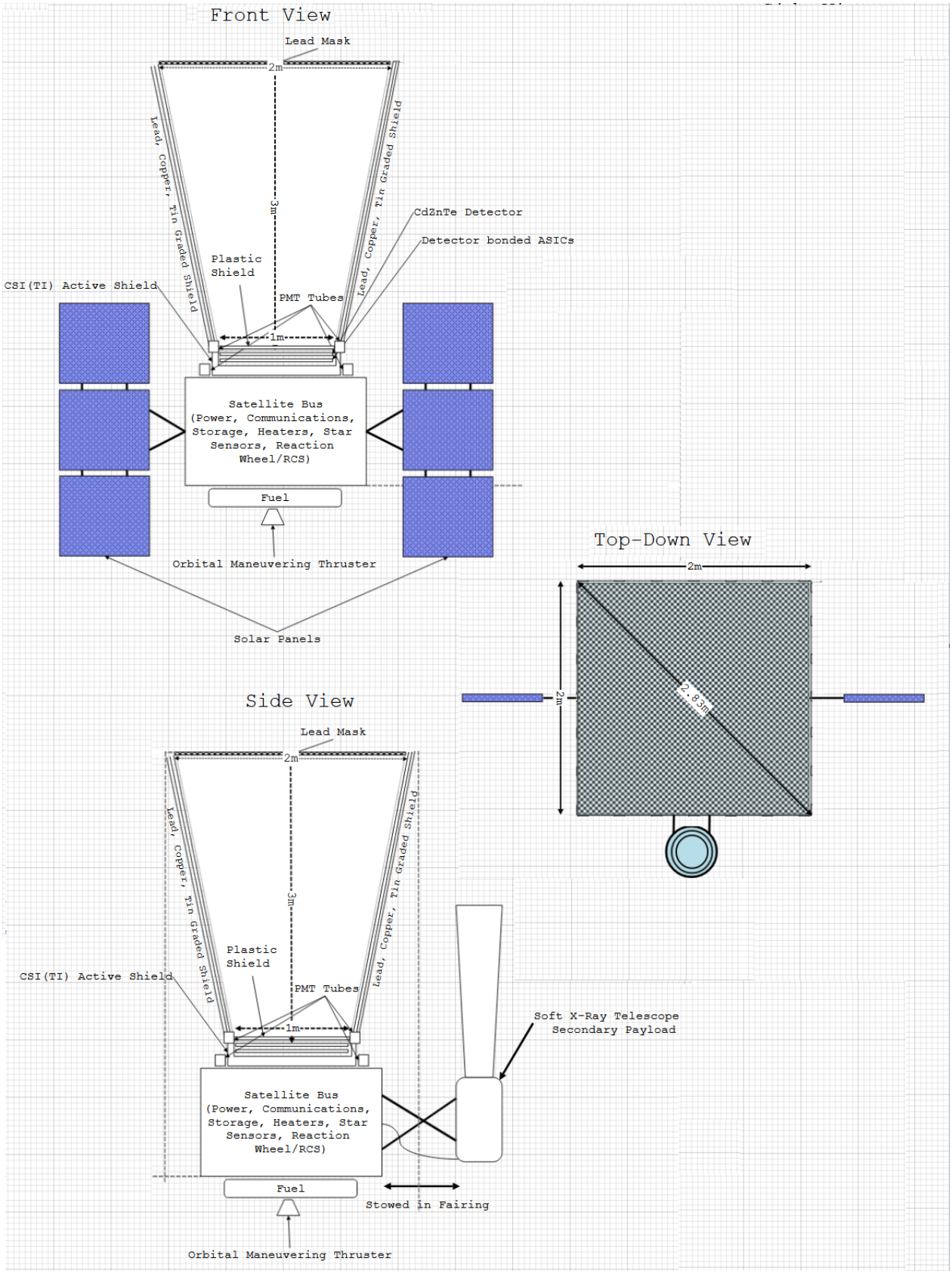

Figure 3: Basic plan of next generation hard x-ray telescope, showing size and ratio of mask and detector distance and sizes.

Semi-conductor detectors, such as CZT, have many advantages compared to other x-ray imaging techniques. They offer a very high energy resolution compared to scintillator detectors, due to the semi-conducting nature of the material. When a hard x-ray photon collides with the semi-conductor crystal it generates a large number of electron-hole pairs, which move under the influence of an externally applied magnetic field. The energy used to move the electrons causes a detectable drop in voltage that is measured. The characteristics of a semi-conductor which make a good gamma ray detector are the band-gap and the operating temperature. The lower the band-gap the higher the energy resolution but also the lower the required operating temperature, as the easier it is for thermal electrons to cross the band-gap.

The current semiconductor with the best band-gap energy is Germanium (0.73eV), but which requires an operating temperature of 77K. For a space-based detector this would require heavy, power-hungry mechanical coolers which is hard to justify unless spectral resolution is critical. Cadmium Telluride is an alternative semiconductor with a higher band-gap (1.44eV) but which can operate at room temperature. The semiconductor used in this detector, Cadmium Zinc Telluride is Cadmium telluride doped with zinc in the ratio $CdZn_xTe_{1-x}$ where x ~0.1, which gives it a slightly higher band-gap energy of 1.57eV. (For a review of the properties of CdTe and CZT see Del Sordo et al., 2009.) CZT typically has a higher resistivity of 1-2 orders of magnitude when compared to CdTe, which results in a proportionally lower leakage current. The energy ranges semiconductors are sensitive in depends on their linear attenuation coefficient μ, which is normally given in a density independent form as a mass attenuation coefficient $\frac{\mu}{\rho}$ where ρ is the density of the object. The fraction of the photons of energy E_γ that are absorbed in a material with a linear attenuation coefficient μ and thickness x is given by

$$\epsilon(E_\gamma) = 1 - e^{-\mu E_\gamma x} \tag{1}$$

The high Z numbers of semi-conductors give them high densities, which translates to a high linear attenuation coefficient, meaning they work better at high energies when compared with other types of detector. Historically the biggest problem with CdTe and CZT detectors has been growing chemically and structurally perfect crystals of a useful volume. This inhibited the practical applications for many decades, but in the last 20 years or so many manufacturing problems were solved, making the growth of larger CdTe and CZT crystals possible. CdTe and CZT detectors both suffer from charge trapping problems, which is due to electron/hole pairs becoming trapped in the crystal, so the full signal is not measured and the spectra peaks show a characteristic tail where the full signal has been impaired. This defect can mostly be accounted for, as a measurement of the rise-time will depend on the degree of charge trapping which allows for the pulse height to be reconstructed. CdTe also suffers from a 'polarisation effect', (see Malm and Martini, 1974) where the performance of the detector is reduced after the detector has been used, due to the trapping and de-trapping of charge carriers changing the electric field distribution in the detectors. It causes a decrease in counting rate and efficiency, and can be minimised using a high voltages and low temperature operation, but these both have downsides. High voltages will increase the leakage current, increasing noise, and low temperature operation means you would need a heavy, power-hungry cooler, and you no longer have the room-temperature operation that is the main advantage of using CdTe over Germanium. According to Del Sordo et al., 2009, CZT does not suffer from the same issue.

The main disadvantages of CZT include a poor ratio of hole and electron mobility lifetime products ($\mu_h\tau_h$ and $\mu_e\tau_e$) due to charge trapping, which limits the maximum thickness and energy response of the crystal, but overall CZT is still a suitable material for for use this in detector.

The 4 companies that produce high quality CZT crystals are eV Products, Imrad, Eurorad and Redlen Technologies. A balloon flown mission called protoEXIST, which was a precursor to a proposed mission called EXIST (Hong et al., 2010, Grindlay et al., 2010) used 2cm x 2cm x 0.5cm CZT crystals from Redlen Technologies, grown using a travelling heater technique which produced high quality, cheap CZT crystals. These crystals are of a comparable volume to the ones proposed for this telescope. The arrangement of the read-out contacts in pixels allows a single continuous crystal to act as an imaging detector, with a high spatial resolution. Each crystal will be read out by a directly bonded application specific integrated circuit (ASIC) which consumes less than $100\mu W$ per pixel. (Hong et al., 2009). These ASICs were developed by a company called RadNet, and are based on an ASIC originally designed for HEFT (Hong et al., 2006). This allows for a large number of pixels with a low power consumption, which is critical for a space-based telescope. The downside of an ASIC with such a low power consumption is a lower spectral resolution

(protoEXIST had around 3keV), which makes the telescope less suited to high resolution spectroscopy. The predicted spectral resolution is around 5% at 100keV, which while better than can be achieved with other x-ray imaging techniques, is worse than has been achieved with comparable CZT and CdTe (see Del Sordo et al., 2009).

The use of pixelated crystals allows for a large sensitive area with high spatial resolution. The large area is critical for producing a sensitive detector, as the sensitivity grows with the square root of the area, and the small pixels mean the telescope has a good point source location accuracy. This combination allows the telescope to detect very faint sources, which is critical when observing high redshift AGN, and to locate them to a high degree of precision, so they can be matched to sources in other bands. If you designed a telescope with a much higher sensitivity than current generation telescopes, like INTEGRAL or Swift, but with a similar angular resolution, the problem of source confusion would become much more apparent, because you would be able to detect more sources, meaning the average angular distance between sources would decrease, and you would struggle to distinguish between sources. This design should mitigate this by improving the angular resolution and PSLA when compared to current generation telescopes. The telescope will have a focusing soft x-ray telescope as a secondary payload, which will conduct simultaneous observation with a greater angular resolution in order to identify the hard x-ray targets in the soft x-ray band.

The major limiting factor historically in the number of channels in a space-based x-ray detector is the power consumption and dissipation requirements. Each readout channel requires it's own electronics, and while the power each channel uses is not a lot, when you are talking about tens to hundreds of thousands of channels, it adds up quickly. This is a problem for several reasons. Firstly, the power to operate all these electronics must come from somewhere, either the solar panels or batteries. If you have a high readout power, you will require a lot of solar panels, and if you are in earth orbit you will also need a lot of batteries for when you can't see the Sun. Batteries are very heavy and increasing the area of solar panels needed increases the complexity of the deployment mechanism needed to fit them inside the launcher. Secondly, the telescope will be required to dissipate the vast majority of the input power as a form of waste heat. It is very hard to dissipate heat in space, as all dissipation has to be done via radiation. This typically requires a radiator with a large surface area. Swift-BAT, which had 32,000 CZT detectors, had to dissipate around 200W of heat using a $1.4m^2$ radiator (Barthelmy et al., 2005). That works out to around 6 mW per channel for Swift-BAT. The ASICs proposed for use here have been demonstrated to use only 100 μW per channel, allowing a much greater a number of channels while also requiring less power than Swift-BAT. The power dissipation required for the readout electronics for XBEX is <100W.

Due to the complexity and density of the electronics readouts, although the total power dissipation required is not unreasonable, it may be harder than normal to efficiently extract heat from the detector plane. In light of this, 20W of power and 100kg of extra mass have been allocated for further cooling solutions if deemed necessary, such as a closed cycle heat pump or radiator, to ensure that the detector can continue to operate at its optimum temperature.

4.2 Imaging System

The imaging system will implement a coded mask design, where 50% of the mask is opaque, and 50% is transparent. This mask pattern uniquely encodes the source information, called convolution, which can the be decoded (deconvoluted) using several different software algorithms, such as back projection, cross correlation, maximum likelihood and maximum entropy.

A coded mask telescope was chosen because they can have a wide FOV with good angular resolution, making them suitable for survey telescopes. Coded mask telescopes also have the property of having a much better point source location accuracy than the angular resolution, which is useful for precisely locating sources in hard x-ray. They also operate over a broad energy range and have a reasonable efficiency. Focusing x-ray telescopes, such as NuSTAR, and proposed designs using Laue lenses generally have better sensitivity, but only work at lower, or specific, energies. They also have very small FOVs, making them unsuitable for use in a all-sky survey telescope. The pixels that make up the mask must be larger than or equal to the size of the detector pixels. A twin-prime uniformly redundant array based mask is optimal because every object position is encoded uniquely on the detector, meaning that the auto-correlation pattern of the mask will be a delta-function, with no side-lobes. Random masks are much easier to design but generally

Energy Range (keV)	FCFOV (°)	HCFOV (°)	PCFOV (°)	Angular Resolution (')	PSLA (5σ source) (")
10 - 300	18.9	36.0	53.3	3.4	13.8

Table 1: Telescope capabilities, including the field of view with different amounts of coding, the angular resolution and the point source location accuracy.

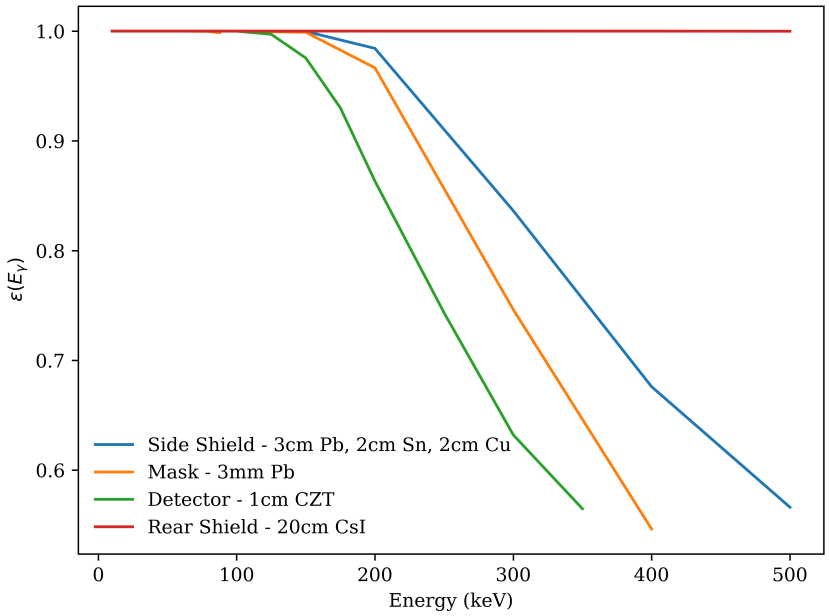

Figure 4: Graph showing the detection/absorption efficiency for the detector, mask, side shield and rear shield as a function of photon energy. Calculated from the material thicknesses given above, and mass attenuation coefficients taken taken from Hubbell and Seltzer, 1995.

have noisy side-lobes. The use of a URA mask requires that the mask be a repeat of a basic mask pattern, with the same geometrical area as the detector. The mask will have 4× the area of the detector, meaning that the mask will consist of a 4x repeated unit pattern.

The telescope will use a Twin Prime URA coded mask, made of lead, positioned 300cm in front of the detector. It will have pixels of 3mm x 3mm, and a thickness also of 3mm. The mask itself will be 200 cm by 200cm, which gives the mask-detector area ratio of 4 needed to use a non-random mask. This gives the mask an area of 40,000cm^2, and a mass of ~ 70 kg. The use of lead over another high-z material, such as tungsten, is due to the optimisation of the telescope below 200keV, for which 3mm of lead attenuates 97% of incident photons.3mm x 3mm mask pixels gives a sampling ratio of 3, which is enough to have a close to ideal sensitivity (see Figure 35 A. Bird, 2020). 3mm thick lead pixels are the thickest that are possible with the size of mask pixel we have, as if mask pixels are thicker than they are wide they can start to act as a collimator, and attenuate off-axis flux. For this design flux is only attenuated when incident at greater than 45°, which means that the flux is unattenutated inside the fully-coded field of view (FCFOV), and half coded field of view (HCFOV).

The design has a FCFOV of 18.9 °by 18.9 °, a HCFOV of 36.0°and a PCFOV of 53.3°. This is a much larger field of view that INTEGRAL, allowing the telescope to see more of the sky at a time, which reduces the total number of exposures needed to cover the whole sky, increasing the amount of time that can be spent observing each part of the sky. The mask pattern itself has not been specifically designed here, but will be outlined in a followup paper.

4.3 Shielding

The telescope will employ 3 separate shielding techniques. Behind and to the sides of the detector there will be a 20cm thick Thallium-activated Caesium Telluride (CsI(TI)) shield, surrounded by photo-multipliers,

acting as an active veto detector. Any detection in the detector which is concurrent with a detection in the veto shield is likely a spurious detection, and will be discarded. CsI(TI) was chosen over Bismuth Germanate (BGO) because BGO has a lower light output, meaning that low energy (<150keV) interactions might not be detected. CsI(TI) also suffers from this problem, but to a lesser degree - it has a veto threshold around 100keV (A. Bird, 2020). The active rear shield also shields against charged particle background.

The inverted pyramidal frustum that makes up the walls between the detector and mask will be made of a graded shield of Lead, Tin and Copper. This was chosen to act as a passive shield because many of the particles that come through the sides of the telescope will not go through the detector, and so using an active veto shield there would only needlessly increase downtime. The components of the graded shield were chosen because they constitute high-Z, medium-Z and low-Z materials, where high energy photons are absorbed in the first shield, which fluoresces a lower energy photon, which is absorbed in the next layer of shield, and so on. The last layer of shield produces photons below the energy range of the detector, meaning they don't contribute to the background. The thickness of the graded shield is 3cm of lead, 2cm of tin and 2cm of copper. The last technique consists of a plastic shield and associated photomultiplier tubes just in front of the detector to stop charged particles interfering with the detector. The plastic does not attenuate hard x-rays, but will stop charged particles like electrons and protons very effectively.

CSI(TI) has a slow decay, meaning that it can become saturated at high count rates, as one pulse has not fully decayed before the next one starts (see Photonics, 2000). This would be a problem in this detector due to the very large size of the CSI(TI) active shield. For simplicity the mass of the shield has been calculated as one uniform object, but in reality it would be made up of many individual CSI(TI) crystals and photo-multiplier tubes, to account for the slow decay problem, and the maximum size of CSI(TI) crystals. I estimate around 50 10-15cm diameter PMT tubes will be necessary, each weighing around 250g, for a total of 12.5kg. This covers around 10% of the surface of the scintillator. The rest of the outside surface of the scintillator will be covered in highly reflective coating, to ensure as many of the photons as possible make it to the PMTs.

Figure 4 shows the detection/absorption efficiency of the detector and the shielding components discussed above. It is clear how the telescope has been optimised to work under 300keV, as at greater energies the efficiency of the shielding declines.

4.4 Secondary Instruments

The proposed secondary payload is a soft x-ray telescope, sensitive between around ~1-10keV. It will be of a focusing design, using grazing-incidence optics and a CCD chip. It is likely to be a successor to the Swift-XRT (Burrows et al., 2005) telescope, which worked between 0.2 and 10 keV, with a 23.6' × 23.6' field of view, or the ISRO's AstroSat-SXI instrument (Tsunemi et al., 2016). It will have a smaller field of view and higher sensitivity than the main telescope, and will be used to match sources between the soft and hard x-ray bands. This will allow the determination of a more accurate source location, and the soft x-ray observations are also useful to estimate the column density of N_H in absorbed and Compton-thick AGN. The soft x-ray telescope will also be able to observe the 6.4keV fluorescent line emission, which is an indicator of an absorbed AGN, as it comes from the gas in the obscuring torus. The secondary payload has been allocated a generous 500kg, 100W and 300kbps mass, power and telemetry budget, which should be more than enough for a very capable soft x-ray telescope - for comparison NuSTAR weighed only 350kg at launch.

5 Mission Profile

Aiming for a launch in late 2027 on an Ariane 6.2 from Kourou, French Guiana. The mission will be a piggyback mission as the payload capacity of the Ariane 6.2 is too large for a single LEO launch. The telescope will spend the first few months in orbit running calibrations and test observations, and then will begin its 3 year survey in the first quarter of 2028. The spacecraft will be carrying consumables sufficient for a 5 year mission, including fuel for boosting the orbit to account for orbital decay.

Science Payload Components	Mass (kg)
Electronics Systems	100
Power supplies	25
Optical star sensors	30
Heaters	25
Mask support structure	100
Detector - Crystals	58
Detector - Readout Electronics	58
Detector Cooling/Radiator	100
Secondary Payload	500
CSI(TI) Rear Shield	734
Rear Shield PMTs	10
Plastic Shield	21
Plastic Shield PMTs	2.5
Graded Passive Shield	1213
20% structure	609
Total	**3653 kg**

Table 2: Table showing science payload mass breakdown.

5.1 Orbital Information

The spacecraft will be placed into a LEO, zero inclination, orbit, with an apogee of around 600km. This was chosen to afford the spacecraft most of the protection from the Earth's magnetic field while not passing through the high levels of radiation in the Van Allen belts. According to Ganushkina et al., 2011, the Van Allen belts typically start above 1000km above Earth's surface, apart from above the South Atlantic anomaly, where they can dip as low as 200km. The 600km orbit also ensures that the spacecraft experiences less orbital decay, to ensure a nominal mission lifetime of 5 years is possible. The inclination of 0° was chosen so the spacecraft can avoid the higher background noise caused by the South Atlantic anomaly. This is a similar height to the Swift spacecraft, which orbits in a ~550km orbit, but with an inclination of 22°. The Swift satellite has maintained it's orbit for 16 years at the same altitude, so orbital decay is not expected to have a major impact on the lifetime of the mission. The zero inclination orbit means that the spacecraft can stay operational and observing for the vast majority of its orbit. This is essential for a survey telescope, as it ensures as efficient as possible use is made of the instrumentation. The uptime is expected to be > 90%, with the only possible time the spacecraft needing to switch off being when it passes north of the SAA. For example, the Swift observatory averaged a 92% uptime while also passing through the SAA regularly (see Oh et al., 2018). The approximate 90 minute orbit will cause more thermal cycling than other orbits, where the outside temperature of the satellite will change quickly as the satellite moves in and out of eclipse, but the standard use of space-rated materials and construction techniques, and the heating and cooling systems built in to the satellite will ensure this will not impact the observations. The spacecraft also spends more time in eclipse, meaning the power available in this time is lower, but this is more than offset by the massively decreased power use for telemetry compared to that which is required in an HEO or L2 orbit. This will allow the spacecraft to downlink all its observations (photon-counting mode), and no data compression will be required on the spacecraft.

5.2 Mass, Power and Telemetry Budgets

5.2.1 Mass Budget

The Ariane 6.2 rocket has a total payload capacity of 10,000 kg to an i=0°orbit. From this 10,000kg, 939kg will go towards basic spacecraft systems such as power supply and generation, attitude control, telemetry, and the general structure of the spacecraft. This includes an extra 80kg for telemetry, to support the increased size of the antenna used to increase the downlink speed, a slight increase in solar array mass

Subsystem	Basic Mass (kg)
Power	95
Solar Array	54
Attitude Control (AOCS)	90
Telemetry (TCMS + DH)	120
Reaction Control (RCS)	55
Structure	250
Thermal	35
Harness	40
Extra Fuel	200
Total	**939**

Table 3: Table showing mass budget making up the basic spacecraft systems

to account for a 20% increase in power generation, and an extra 200kg of fuel, to correct for orbital decay caused by drag and extend the mission lifetime. These are detailed in Table 5.2.1. 100kg of fuel will go towards correcting the orbit, as the orbit the Ariane 6.2 delivers the rocket to is not precisely the correct orbit needed. 4500kg goes towards a second payload, as this reduces the cost of the mission by sharing the cost of the rocket with another party, and still provides ample mass for both missions. There is also further science payload specific components including electronics and harnesses, power supplies, optical star sensors, heaters and a mask support structure. These are detailed in Table 5.2.1, along with the masses of the various detector components.

The detector mass is calculated from the thickness of the detector (1cm), the area of the detector (10,000 cm^2) and the density of CZT (5.8 g/cm^3), and the mass of the electronic readout components are taken to be the same mass, which is likely an overestimate. The extra cooling mechanisms to extract heat from the electronics plane are estimated as 100kg. The secondary payload, which is a soft x-ray telescope, is estimated as 500kg. The mass of the CSI(TI) shield is calculated in a similar way to the mass of the detector. The photo-multipliers are estimated as 0.25 kg each, and a total of 50 are estimated to be necessary to cover 10% of the surface of the active shields. The graded passive shield mass is estimated from the surface area of the pyramidal frustum multiplied by the thicknesses and densities of each shield component. Overall the current design, including the science and spacecraft systems weighs 4592 kg, which is within the 5400kg total payload capacity for science and s/c components.

The available height in the top section of the Araine 6.2 payload fairing is 10.6m, of which 2.74 is straight and the rest slowly tapers into a cone. The available diameter is 4.7m. The widest part of the spacecraft, as can be seen in figure 3, is the mask, which at 2m a side has a longest distance of ~2.83m. The distance between the mask and the detector is 3m, and the detector and spacecraft body itself should be no more than another 2m, so from this we can conclude the spacecraft will easily fit into the payload fairing with room to spare. The secondary payload is shown as being deployed from the side of the spacecraft and extending, but depending on the final size of the secondary telescope it may be able to be launched extended already. If it has to be launched retracted, this risk is mitigated by using a very simple deployment mechanism, which only has to work once, and if it didn't work, would not affect the main science payload.

5.2.2 Telemetry Budget

The base transmission rate for the standard antenna in LEO is 433kbps. The antenna is non-directional, and will be transmitting to ground constantly, but with limited on-board backup. The maximum total counts were found by fitting the background counts to a power-law, and integrating background counts cm^{-2} s^{-1} keV−1 over the total area of the detector, 10,000 cm^2, and over the energy range of the detector, which in this case was taken to be 10 - 500 keV. The source counts were then taken from the power-law emission of the Crab Nebula, which is one of the brightest x-ray sources in the sky. The approximate power-law emission of the Crab Nebula is given in A. Bird, 2020 as

$$F(E_\gamma) = 9E_\gamma^{-2.14} photons\, cm^{-2}\ s^{-1}\ keV^{-1} \tag{2}$$

Subsystem	Basic Power (W)	
	Sun	**Eclipse**
Attitude Control (AOCS)	121	120
Reaction Control (RCS)	0	0
Telemetry (TCMS + DH)	24	24
DH	61	61
Power	30	42
Thermal	96	96
Payload	320	278
Contingency	194	79
Total	846	700

Table 4: Table showing the power requirements of the spacecraft, in both eclipse and solar illumination.

This was also integrated over the 10-500keV range, and over the area of the detector to produce a total counts/s for the source. The actual sources that will be observed will be a lot fainter, and the count rates are likely to be much lower as well. With a 20% margin of error, the total counts per second was calculated to be 15,000 cts/s. The number of bits needed to represent one count depends on the spatial, timing and energy sensitivity of the detector. With 1Mpix of pixels, each pixel can be represented by an x-y coordinate. This means a total of 20 bits are used to indicate position. The timing resolution of this telescope is not particularly high, as the observational targets are so faint, so it was taken as specifying to 0.1s accuracy over a 10 year period. This came to a total of 18 bits to specify timing. The energy resolution of the detector, while good, is not exceptional so 10 bits for energy resolution was chosen, meaning a total of 1024 energies can be transmitted, which is more than enough for the energy resolution of the detector. This comes to a total of 48 bits per detection, which when multiplied by the count rate suggests a need for around 800 kbps. This is just under double the base antenna transmission rate, which can be scaled linearly in mass and power. To allow a sensible margin for error, plus to include some downlink capacity for the secondary payload, a down-link of 1.2 mbps will be provided, and the antenna mass and power consumption have been scaled accordingly. This will also mean an increase in uplink capacity to 9 kbps. The antenna power will then be 24W, and the mass has been scaled to 120kg.

5.2.3 Power Budget

The power generation is provided by deployable solar arrays, along with on-board batteries when the satellite is in eclipse. Table 5.2.3 shows the general power requirements for normal operation of the telescope itself, including for attitude control, telemetry, power distribution, thermal control and the satellite computer, along with the power budget for the science payload itself. Important changes from the default configuration include an increase in telemetry power, taken from decreasing the available science payload power, to increase the downlink capacity of the satellite antenna. The breakdown of the science payload power budget is detailed in Table 5.2.3. As detailed in Section 4.1, each detector virtual pixel uses 100 μW of power, or alternatively each crystal/ASIC pair uses 22.5mW. This gives a total of 100W of power for the detector. However due to the density of the pixels and electronics, some extra power has been dedicated to run a closed-cycle cooler and radiator to extract heat from the electronics plane, to ensure the detector can operate at its optimum temperature. There is also power to run the on-board science computer that handles the data from the detector. The active shielding in the telescope, in both the rear CSI(TI) shield and the front plastic shield, use photo-multiplier tubes, and the power for these is shown in the table. 50 PMTs are estimated to be needed, with each one requiring (a high estimate) of 40mW of power.

Overall the power consumption of the telemetry downlink has been increased, to increase the downlink capacity and ensure the detector can operate in photon-counting mode and send every detection to the ground. The power generation and mass of the solar panels have also both been increased by 20% to allow for this while also keeping a healthy margin of contingency power. These changes are accounted for in table 5.2.3.

Payload	Basic Power (W)	
	Sun	**Eclipse**
Detector readout electronics	100	100
Science Computer	40	40
Photo-multiplier tubes	10	10
Secondary payload	100	100
Detector heat dissipation	20	20
Contingency	50	8
Total	**320**	**278**

Table 5: Table showing power requirements of the science payload, in both eclipse and solar illumination.

5.3 Observing Strategy

The telescope will conduct a uniform all-sky survey, with the sky being split into a grid of 32 equally-sized areas (with a small amount of overlap), allowing the telescope to view the whole sky (in its half coded field of view.) XBEX will be view the whole sky partially coded in around 41 hours for a time of 10^4s per observation. Half-coded it will take ~88 hours to observe the whole-sky. It will take around 1 year to observe the whole sky at a integration time per area of 10^6s (using the HCFOV), and the total integration time (for each area) after 3 years will be around 2.7×10^6s. These calculations assume the telescope is operational for 90% of the time, which is likely an underestimate.

The telescope will observe the whole sky to some degree every 41 hours, but there will be a target of opportunity (ToO) policy covering unpredictable and generically predictable targets of opportunity that will be considered on an individual basis. If the observation can be made within the pointing limitations of the satellite (such as solar array orientation), and the visibility of the target at that point in the orbit, then the order of observations can be changed to observe the ToO sooner than it would otherwise be observed. If the uptime of the telescope is greater than 90%, as is anticipated, this extra time can be used for specific observations and ToO's. This applies to both the main and secondary instruments. The survey and raw data collected will be published regularly and will be available to the astronomical community. Collaborations with other x-ray telescopes, such as INTEGRAL/Swift and NuSTAR are anticipated, as these can eliminate much of the statistical noise from the observations, as discussed in section 3. Collaborations with future telescopes, such as the Wide Field Infrared Survey Telescope (WFIRST), and the James Web Space Telescope (JWST), which can both operate in the infra-red spectrum, would also be possible, as observations of galaxies in IR can be used to detect accreting AGN, as is detailed in section 3.

As discussed in 3, the sensitivity of the 3 year all-sky survey will be around $9 \times 10^{-13}\, ergs^{-1}cm^{-2}$, which suggests we will detect around 10,000 sources, including 700-2000 Compton-thick AGN. This is an order of magnitude more than have currently been discovered (see Krivonos et al., 2012 and Bird et al., 2016), and will allow investigation of the various science goals discussed previously, including proportion of AGN which are Compton-thick, resolving more of the point sources than make up the hard x-ray background, and determining whether the proportion of Compton-thick AGN changes with redshift. It is not unreasonable to hope that the XBEX mission will continue beyond the original 5 year plan, when compared with similar missions such as Swift, which has been operating in a similar orbit since 2004. If XBEX is still operational after its 3 year survey, it will conduct specific pointings on targets of interest identified during the 3 year survey, and proposals for dedicated observing slots will be considered via an Announcement of Opportunity and peer review.

6 Telescope Performance

In section 3.5, I laid out some science-based requirements for XBEX. The first requirement was to look at the whole sky as often as possible, ideally every day. The current observing pattern for the telescope allows it to look at each region of the sky, half-coded, for 10^4s, every 41 hours. This requirement has mostly been met, but given the field of view of the telescope and a reasonable integration time for each image, looking at

the whole sky every day would not have been possible. The field of view was set as a compromise between angular resolution and the time required to view the whole sky. This has a limited impact on the science goals, it makes the telescope slightly less suitable for observing AGN with short-period variability, and for observing new transitory sources, but neither of these are critical for the main science goals of the mission.

The second science requirement was around sensitivity. Here the telescope exceeded the requirement, which was derived based on a target number of AGN sources, and to survey at a greater sensitivity than previous missions, and was hence set as 1×10^{-12} $erg\ s^{-1}\ cm^{-2}$. The conversion between a sensitivity in these units and a continuum sensitivity in $phs^{-1}cm^{-2}keV^{-1}$ is non-trivial, and depends on the spectral energy distribution of the observed target and the telescope sensitivity at different energies. The distribution in this case was taken as a canonical AGN with a photon index Γ of 1.7. With this in mind, the derived sensitivity of the all-sky survey for XBEX was found to be 9×10^{-13} $erg\ cm^{-2}s^{-1}$. At this sensitivity we expect to see ~10,000 extragalactic sources, including between 700 and 2000 Compton-thick AGN. The third requirement was that the detector have an angular resolution better than 5'. This was derived from the distribution of sources on the sky, including a margin of error for the other types of sources not considered here but which will be observed, and to have a better angular resolution than previous mission. This target was also exceeded, with a predicted angular resolution of 3.4'. This is because the angular resolution is tied to the point source location accuracy, which was set a more ambitious target.

The fourth requirement was that the point source location accuracy be <30" for a 5σ source. This was set to allow accurate determination of hard x-ray sources in other energy bands. This target was also exceeded, with a predicted PSLA of ~14".

The fifth requirement was around the energy resolution of the detector. The telescope should be able to do spectroscopy, but the continuum sensitivity was considered more important for the science goals. This requirement was not entirely met, due to the PSLA and sensitivity requirements meaning a large number of pixels is required, leading to the selection of very power-efficient readout electronics that aren't as good at energy resolution. However the energy resolution is still predicted to be around 5% at 100keV, which is better than is achieved with other types of detector.

The final requirement was around the secondary payload. This soft x-ray telescope would be able to simultaneously characterise the column density of N_H in the sources being observed in hard x-ray, which is important for identifying the absorption of an AGN. This target was achieved, with allowances being made in the mass, power and telemetry budgets for a soft x-ray telescope sensitive between 0.5 and 10keV.

Overall the telescope meets or exceeds the most critical targets required to undertake its science mission. XBEX would be a very capable instrument that would advance our knowledge of AGN evolution and the hard x-ray background considerably.

6.1 Sensitivity and Background

There are 3 main sources of background noise in a hard x-ray telescope. These are neutron/spallation, aperture leakage and shield leakage. The neutron background comes from neutrons, which aren't all stopped by the shield, interacting in the detector. Spallation induced background is due to high energy protons generating radioactive isotopes within the detector, which decay via β-decay, causing spurious background counts. The counts from these sources depend on the volume of the detector, and the rigidity cutoff, which depends on the orbit the spacecraft is in. A higher rigidity cutoff is better, because it means the Earth's magnetic field stops some of the background from reaching the spacecraft. As the telescope is in a low equatorial orbit, the rigidity value is high (between 11-15 GV), whereas in a HEO it would only be 2GV (see A. Bird, 2020). This translates to around 60% of the total neutron/spallation count (compared to a 4.7GV cutoff), whereas a HEO would receive at least around 130% of the base neutron/spallation background. This decrease in the primary source of background across most of the energy spectrum is one of the reasons a low earth orbit was chosen. The XBEX detector has a very large volume for a gamma-ray detector, of 10,000 cm^3, which means that this source of background dominates at most energies. Decreasing the area or thickness of the detector would decrease the number of background counts from this source, but it would also lower the sensitivity and energy-range of the detector. Aperture leakage is given by

$$B_{CDB}(E_\gamma) = 87.4 \times \epsilon(E_\gamma)E_\gamma^{-2.3}\ \Omega\ counts\ cm^{-2}\ s^{-1}\ keV^{-1} \tag{3}$$

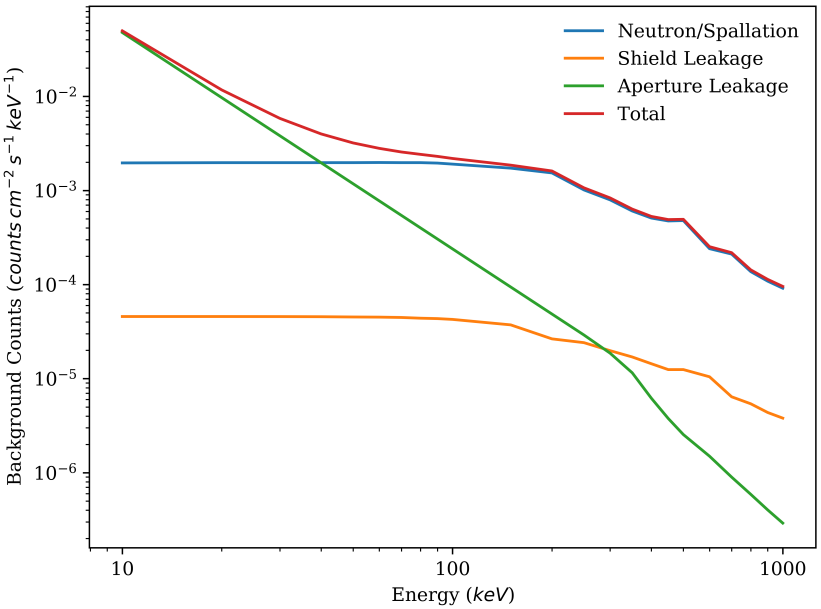

Figure 5: Figure showing total background counts, and the contribution to the total by each of the 3 background components; neutron/spallation, shield leakage and aperture leakage.

where $\epsilon(E_\gamma)$ is the detection efficiency, E_γ is the energy (in keV), and Ω is the solid angle aperture of the telescope (in steradians). This contribution is much higher in a survey telescope than other types of hard x-ray telescope, as survey telescopes tend to have a large field of view. The power index of -2.3 in the background count means that this background source decreases quickly at higher energies, meaning that it only dominates at the lowest energies. The fully coded solid angle aperture of 0.109 sr, a half coded solid angle aperture of 0.395 sr, and a partially coded solid angle aperture of 0.860 sr. The background count from this source could be decreased by reducing the aperture of the telescope, however this would increase the amount of time needed to image the whole sky to a particular sensitivity. If the aperture is reduced too much then the telescope is no longer a all-sky "survey" telescope, as it would weeks to months to survey the whole sky. The current aperture of the telescope is a compromise between reducing the aperture leakage, while keeping an acceptable field of view and angular resolution.

The third background source is shield leakage. This comes from the fact that the shield will not stop all photons at a specific energy - the higher the energy, the thicker the shield needs to be to stop most of the photons. The absorption efficiency for the different parts of the shield is shown above, in Figure 4. The fact that the spacecraft is intended for a low earth orbit means that there is more available payload capacity onboard the Ariane 6.2 rocket; the spacecraft can be heavier. One of the heaviest parts of a hard x-ray telescope is the shielding, and this mission can dedicate a lot more mass than comparable missions towards shielding. The active rear shield is comprised of 20cm of CsI(TI), and has a total mass of ~700kg. This is a very thick shield, and attenuates 90% of incident photons up to 500keV. A thinner shield would be almost as good, and a lot lighter, but the use of a thick shield ensures that shield leakage will be a negligible source of background counts. A CsI(TI) shield also needs to be thicker than an equivalent shield of BGO, due to a lower density. The side shield is made by a graded shield of 3cm of Lead, 2cm of Tin and 2cm of Copper, and weighs ~1200kg. This is does not attenuate photons as effectively as the active rear shield, but it still efficient enough over the energy range the telescope is designed for, and stops ~85% of the photons at 300keV. Overall both shields ensure that the shield leakage will not have a significant impact on the total background. The first two types of background were both dependent on other aspects of the design, and so could not be reduced further without negatively impacting another parameter, but the mass allowance was high enough to significantly reduce the shield leakage without negatively impacting any other design metric.

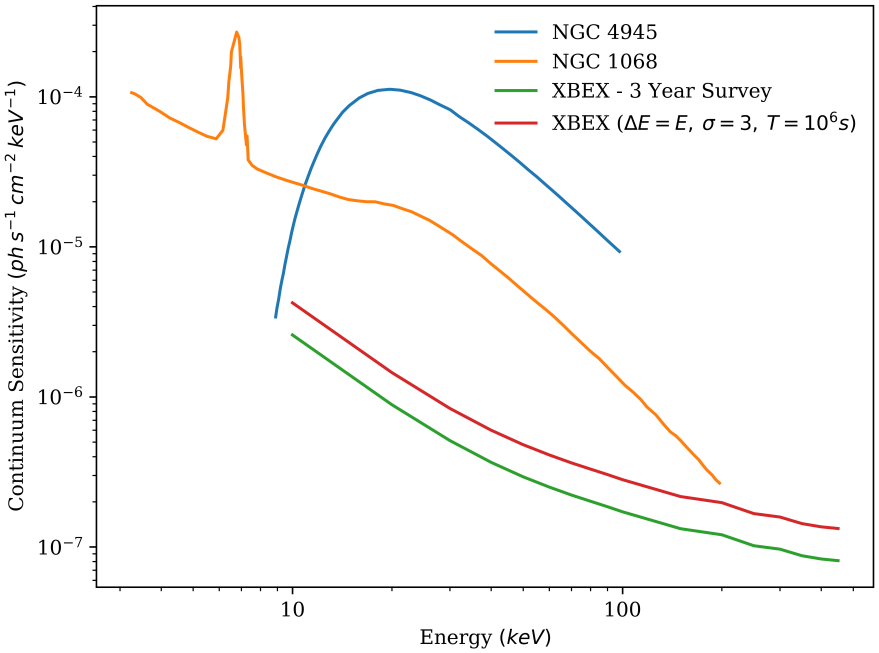

Figure 6: Figure showing the sensitivity of XBEX, for both 10^6s and the 3 year survey, and showing the comparison to two hard x-ray sources, NGC 1068 (Matt et al., 1997) and NGC 4945 (Puccetti et al., 2014), which respectively are examples of heavily Compton-thick and lightly Compton-Thick AGN, as a function of photon energy.

The sensitivity of the coded mask telescope was estimated from the equation

$$F_{min} = \frac{\sigma}{\epsilon(E_\gamma)} \sqrt{\frac{4B(E_\gamma)}{AT\Delta E}}\ ph\ cm^{-2}\ s^{-1} keV^{-1} \tag{4}$$

where $\sigma = 3$, $\epsilon(E_\gamma)$ is the detection efficiency at that energy (seen for this detector in Figure 4), $B(E_\gamma)$ is the background counts ($cts\ cm^{-2}\ s^{-1}\ keV^{-1}$) at that energy (seen in figure 5), A is the area of the detector in cm^2, T is the time of the observation in seconds, and ΔE is the bandwidth over which the measurement is taken (taken here as $\Delta E = E_\gamma$). Figure 6, shows the sensitivity of the telescope from $10 - 400keV$, and a comparison to two sources, NGC1068, and NGC4945. NGC1068 is a heavily Compton-thick AGN ($N_H > 10^{25} cm^2$), and as one of the closest and most well studied AGN, is considered almost an archetypal obscured AGN (see Bauer et al., 2015). NGC4945 is an nearby Seyfert 2 galaxy, and also Compton-thick ($N_H \sim 4 \times 10^{24}\ cm^2$), but to a lower degree than NGC1068. Both of them are easily detected by XBEX in both the 10^6s and 3 year surveys by at least an order of magnitude, and while they are relatively bright sources, XBEX should be capable of detecting much fainter sources that have a similar spectral energy distribution.

Figure 7 highlights how much of a step forward XBEX will be for hard x-ray astronomy. Over the 3 year survey, it will be almost 2 orders of magnitude more sensitive than Swift-BAT, and an order of magnitude better than Integral ISGRI. Between 80 and 300keV it will be the most sensitive hard x-ray instrument in orbit, and while it will not be as sensitive as NuSTAR under 80keV, it will look at a much larger portion of the sky, and so will conduct a much more uniform survey. XBEX will increase the number of both absorbed and unabsorbed AGN that have detected by at least an order of magnitude,and locate them to a greater degree of precision than ever before, allowing us to resolve many more of the individual sources that make up the hard x-ray background.

The most revolutionary part of XBEXs design is the large number of virtual pixels, which will make XBEX the highest resolution hard x-ray telescope ever launched. The use of many small pixels allows for a large detector area, which increases sensitivity, as is seen above, and for very good spatial resolution, which increases the point source location accuracy of the telescope. XBEX has a PSLA (for a 5σ source) of 13.8

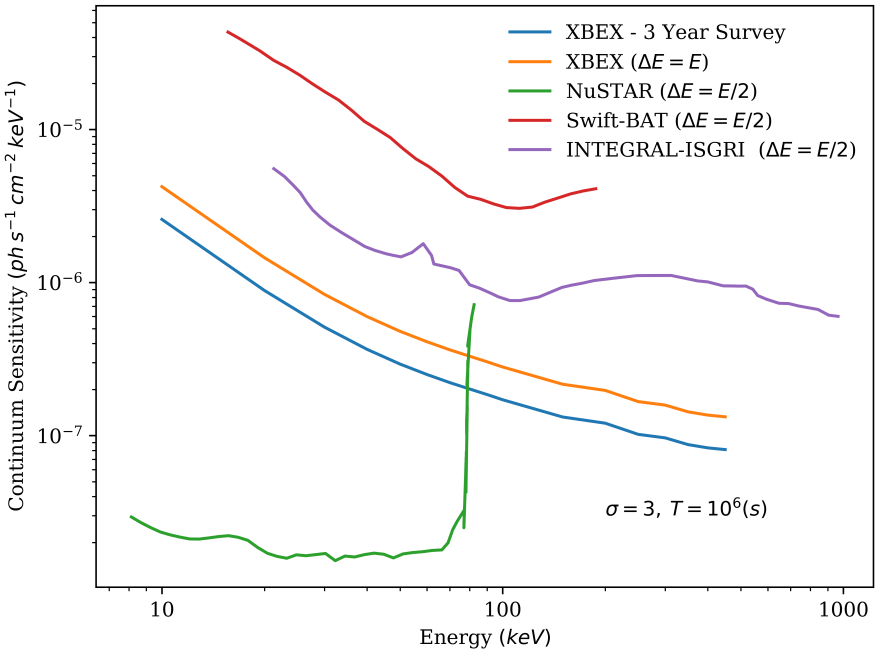

Figure 7: Figure showing the sensitivity of XBEX, for both 10^6s and the 3 year survey, and showing the comparison to INTEGRAL-ISGRI (Lebrun, 2006), Swift-BAT (Grindlay et al., 2010), and NuSTAR (Koglin et al., 2005), as a function of wavelength.

arcseconds, whereas Swift has a PSLA of 1-4 arcminutes (Barthelmy et al., 2005), and INTEGRAL has a PSLA of 1-2 arcminutes (Scaringi et al., 2010). XBEX has almost an order of magnitude better PSLA than Swift or Integral, which will allow hard x-ray targets to be located much more precisely than ever before, making target matching in other energy bands easier and more accurate.

7 Conclusion

This report has outlined my proposal for a new hard x-ray all sky survey telescope, which is currently named the X-ray Background EXplorer, or XBEX. XBEX is a coded aperture telescope, which is based upon the technology applied in the Swift and INTEGRAL missions, but is applied on a much larger scale. The use of over 1 million ”virtual” pixels, allows for an unprecedented spatial resolution, while also achieving an impressive continuum sensitivity. XBEX will work between 10 and 300keV, and will have a 36° by 36° half coded field of view, and an angular resolution of 3.4’. It will have a point source location accuracy of 13.8”, which is very good for a hard x-ray telescope, and makes the identification of hard x-ray sources in other bands much easier and more accurate.

XBEX will study the hard x-ray background, with the mission of resolving much more of the continuum into point sources; as detailed in section 3 less than 1% of the x-ray background above 20keV can be resolved into point sources. XBEX will also study Compton-thick and obscured AGN, to investigate the number density of Compton-thick AGN and to determine whether it is dependent on redshift. XBEX is expected to conduct its 3 year survey down to a sensitivity of $9 \times 10^{-13}\ erg\ s^{-1}\ cm^{-2}$, and to observe over 10,000 new extragalactic sources, including between 700 and 2000 Compton-thick AGN. This will be around 5x more than any previous hard x-ray mission, such as Swift or INTEGRAL. XBEX will also investigate unusual sources such as XBONGs, and will watch the sky for new transient sources.

The design outlined above meets most of the requirements set out in section 3.5, but as with any design, compromises always have to be made. The compromise between the need of both high sensitivity and a good PSLA meant that the energy resolution was compromised slightly, as the readout electronics for the detector, picked for their low power consumption, are a limiting factor in the energy resolution of the

detector. Furthermore the FOV of the telescope is a compromise between the angular resolution and the time it takes to view the whole sky, which resulted in a slightly higher than ideal time to view the whole sky, of 41 hours. This means the telescope will be less effective at studying highly variable AGN that vary significantly on timescales less than a day. However overall the telescope meets or exceeds its most critical goals, including the sensitivity, angular resolution, and point source location accuracy targets, meaning it will be able to complete almost all of its science goals.

XBEX is proposed to launch from in 2027, from Kourou, French Guiana on a Ariane 6.2 rocket as part of a ridesharing program, into a low equatorial orbit. The total science payload mass is ~3650kg, and the total spacecraft mass is ~4600kg. XBEX has a nominal mission lifetime of 5 years, with a 3 year all-sky survey followed by 2 years of pointed observations and time for guest astronomers. XBEX has the potential to revolutionise our understanding of AGN evolution and the x-ray background, and this proposal would launch in time for the retirement of the INTEGRAL satellite, in 2029, and the potential retirement of Swift, to ensure there is a continued dedicated hard x-ray all-sky observational capability for decades to come.

References

A. Bird, N. Segura, S. J. A. D. A. H. T. A. (2020). *Design Course in Gamma Ray Astronomy*. Department of Physics and Astronomy, University of Southampton.

Ajello, M., Alexander, D. M., Greiner, J., Madejski, G. M., Gehrels, N., and Burlon, D. (2012). The 60 Month All-sky Burst Alert Telescope Survey of Active Galactic Nucleus and the Anisotropy of nearby AGNs. , 749(1):21.

Akylas, A. and Georgantopoulos, I. (2019). The source number counts at high energies: Swift vs. nustar. *arXiv preprint arXiv:1902.05137*.

Aleksić, J., Alvarez, E., Antonelli, L., Antoranz, P., Asensio, M., Backes, M., Barrio, J., Bastieri, D., González, J. B., Bednarek, W., et al. (2012). Pg 1553+ 113: five years of observations with magic. *The Astrophysical Journal*, 748(1):46.

Antonucci, R. (1993). Unified models for active galactic nuclei and quasars. *Annual Review of Astronomy and Astrophysics*, 31(1):473–521.

Ballantyne, D. R., Draper, A. R., Madsen, K. K., Rigby, J. R., and Treister, E. (2011). LIFTING THE VEIL ON OBSCURED ACCRETION: ACTIVE GALACTIC NUCLEI NUMBER COUNTS AND SURVEY STRATEGIES FOR IMAGING HARD x-RAY MISSIONS. *The Astrophysical Journal*, 736(1):56.

Baloković, M., Brightman, M., Harrison, F. A., Comastri, A., Ricci, C., Buchner, J., Gandhi, P., Farrah, D., and Stern, D. (2018). New spectral model for constraining torus covering factors from broadband x-ray spectra of active galactic nuclei. *The Astrophysical Journal*, 854(1):42.

Barcons, X., Nandra, K., Barret, D., Den Herder, J., Fabian, A., Piro, L., Watson, M., et al. (2015). Athena: the x-ray observatory to study the hot and energetic universe. In *Journal of Physics: Conference Series*, volume 610, page 012008. IOP Publishing.

Barger, A. J., Cowie, L. L., Mushotzky, R. F., Yang, Y., Wang, W.-H., Steffen, A. T., and Capak, P. (2005). The cosmic evolution of hard x-ray-selected active galactic nuclei. *The Astronomical Journal*, 129(2):578–609.

Barthelmy, S. D., Barbier, L. M., Cummings, J. R., Fenimore, E. E., Gehrels, N., Hullinger, D., Krimm, H. A., Markwardt, C. B., Palmer, D. M., Parsons, A., et al. (2005). The burst alert telescope (bat) on the swift midex mission. *Space Science Reviews*, 120(3-4):143–164.

Bauer, F. E., Arévalo, P., Walton, D. J., Koss, M. J., Puccetti, S., Gandhi, P., Stern, D., Alexander, D. M., Baloković, M., Boggs, S. E., Brandt, W. N., Brightman, M., Christensen, F. E., Comastri, A., Craig, W. W., Moro, A. D., Hailey, C. J., Harrison, F. A., Hickox, R., Luo, B., Markwardt, C. B., Marinucci, A., Matt, G., Rigby, J. R., Rivers, E., Saez, C., Treister, E., Urry, C. M., and Zhang, W. W. (2015). NuSTARSPECTROSCOPY OF MULTI-COMPONENT x-RAY REFLECTION FROM NGC 1068. *The Astrophysical Journal*, 812(2):116.

Bird, A. J., Bazzano, A., Malizia, A., Fiocchi, M., Sguera, V., Bassani, L., Hill, A. B., Ubertini, P., and Winkler, C. (2016). THE IBIS SOFT GAMMA-RAY SKY AFTER 1000 INTEGRAL ORBITS. *The Astrophysical Journal Supplement Series*, 223(1):15.

Bottacini, E. and Ajello, M. (2012). Combining the Swift/bat and the Integral/isgri Observations. In *Astroparticle*, pages 25–28.

Bottacini, E., Ajello, M., and Greiner, J. (2012). The Deep Look at the Hard X-Ray Sky: The Swift-INTEGRAL X-Ray (SIX) Survey. , 201(2):34.

Brusa, M., Civano, F., Comastri, A., Miyaji, T., Salvato, M., Zamorani, G., Cappelluti, N., Fiore, F., Hasinger, G., Mainieri, V., Merloni, A., Bongiorno, A., Capak, P., Elvis, M., Gilli, R., Hao, H., Jahnke, K., Koekemoer, A. M., Ilbert, O., Floch, E. L., Lusso, E., Mignoli, M., Schinnerer, E., Silverman, J. D., Treister, E., Trump, J. D., Vignali, C., Zamojski, M., Aldcroft, T., Aussel, H., Bardelli, S., Bolzonella, M., Cappi, A., Caputi, K., Contini, T., Finoguenov, A., Fruscione, A., Garilli, B., Impey, C. D., Iovino, A., Iwasawa, K., Kampczyk, P., Kartaltepe, J., Kneib, J. P., Knobel, C., Kovac, K., Lamareille, F., Leborgne, J.-F., Brun, V. L., Fevre, O. L., Lilly, S. J., Maier, C., McCracken, H. J., Pello, R., Peng, Y.-J., Perez-Montero, E., de Ravel, L., Sanders, D., Scodeggio, M., Scoville, N. Z., Tanaka, M., Taniguchi, Y., Tasca, L., de la Torre, S., Tresse, L., Vergani, D., and Zucca, E. (2010). THEXMM-NEWTONWIDE-FIELD SURVEY IN THE COSMOS FIELD (XMM-COSMOS): DEMOGRAPHY AND MULTIWAVE-LENGTH PROPERTIES OF OBSCURED AND UNOBSCURED LUMINOUS ACTIVE GALACTIC NUCLEI. *The Astrophysical Journal*, 716(1):348–369.

Burrows, D. N., Hill, J., Nousek, J. A., Kennea, J. A., Wells, A., Osborne, J., Abbey, A., Beardmore, A., Mukerjee, K., Short, A., et al. (2005). The swift x-ray telescope. *Space science reviews*, 120(3-4):165–195.

Comastri, A., Gilli, R., Vignali, C., Matt, G., Fiore, F., and Iwasawa, K. (2007). Compton Thick AGN in the Suzaku Era. *Progress of Theoretical Physics Supplement*, 169:274–277.

Cusumano, G., La Parola, V., Segreto, A., Ferrigno, C., Maselli, A., Sbarufatti, B., Romano, P., Chincarini, G., Giommi, P., Masetti, N., Moretti, A., Parisi, P., and Tagliaferri, G. (2010). VizieR Online Data Catalog: The 54-month Palermo BAT-survey catalogue (Cusumano+, 2010). *VizieR Online Data Catalog*, pages J/A+A/524/A64.

Del Sordo, S., Abbene, L., Caroli, E., Mancini, A. M., Zappettini, A., and Ubertini, P. (2009). Progress in the development of cdte and cdznte semiconductor radiation detectors for astrophysical and medical applications. *Sensors*, 9(5):3491–3526.

Draper, A. R. and Ballantyne, D. R. (2010). The Evolution and Eddington Ratio Distribution of Compton Thick Active Galactic Nuclei. , 715(2):L99–L103.

ESA (2015). Integral manoeuvres for the future. Technical report, ESA.

Fabian, A., Barcons, X., Almaini, O., and Iwasawa, K. (1998). Do nuclear starbursts obscure the x-ray background? *Monthly Notices of the Royal Astronomical Society*, 297(1):L11–L15.

Franca, F. L., Fiore, F., Comastri, A., Perola, G. C., Sacchi, N., Brusa, M., Cocchia, F., Feruglio, C., Matt, G., Vignali, C., Carangelo, N., Ciliegi, P., Lamastra, A., Maiolino, R., Mignoli, M., Molendi, S., and Puccetti, S. (2005). The HELLAS2xmm survey. VII. the hard x-ray luminosity function of AGNs up toz= 4: More absorbed AGNs at low luminosities and high redshifts. *The Astrophysical Journal*, 635(2):864–879.

Frank, J., King, A., Raine, D., and King, B. (2002). *Accretion Power in Astrophysics*. Accretion Power in Astrophysics. Cambridge University Press.

Furui, S., Fukazawa, Y., Odaka, H., Kawaguchi, T., Ohno, M., and Hayashi, K. (2016). An x-ray spectral model of reprocessing by smooth and clumpy molecular tori in active galactic nuclei with the monaco framework. *The Astrophysical Journal*, 818(2):164.

Ganushkina, N. Y., Dandouras, I., Shprits, Y., and Cao, J. (2011). Locations of boundaries of outer and inner radiation belts as observed by cluster and double star. *Journal of Geophysical Research: Space Physics*, 116(A9).

García-Burillo, S., Combes, F., Almeida, C. R., Usero, A., Krips, M., Alonso-Herrero, A., Aalto, S., Casasola, V., Hunt, L., Martín, S., et al. (2016). Alma resolves the torus of ngc 1068: continuum and molecular line emission. *The Astrophysical Journal Letters*, 823(1):L12.

Giacconi, R. (2003). Nobel lecture: The dawn of x-ray astronomy. *Rev. Mod. Phys.*, 75:995–1010.

Gilli, R., Comastri, A., and Hasinger, G. (2007). The synthesis of the cosmic x-ray background in the chandra and xmm-newton era. *Astronomy & Astrophysics*, 463(1):79–96.

Grindlay, J., Gehrels, N., Bloom, J., Coppi, P., Soderberg, A., Hong, J., Allen, B., Barthelmy, S., Tagliaferri, G., Moseley, H., et al. (2010). Overview of exist mission science and implementation. In *Space Telescopes and Instrumentation 2010: Ultraviolet to Gamma Ray*, volume 7732, page 77321X. International Society for Optics and Photonics.

Hong, J., Allen, B., Grindlay, J., Chammas, N., Barthelmy, S., Baker, R., Gehrels, N., Nelson, K., Labov, S., Collins, J., Cook, W., Mclean, R., and Harrison, F. (2009). Building large area czt imaging detectors for a wide-field hard x-ray telescope—protoexist1. *Nuclear Instruments and Methods in Physics Research Section A: Accelerators, Spectrometers, Detectors and Associated Equipment*, 605:364–373.

Hong, J., Grindlay, J., Allen, B., Skinner, G., Barthelmy, S., Gehrels, N., Garson, A., Krawczynski, H., Cook, W., Harrison, F., et al. (2010). The proposed high-energy telescope (het) for exist. In *Space Telescopes and Instrumentation 2010: Ultraviolet to Gamma Ray*, volume 7732, page 77321Y. International Society for Optics and Photonics.

Hong, J., Grindlay, J., Chammas, N., Copete, A., Baker, R., Barthelmy, S., Gehrels, N., Cook III, W., Burnham, J., Harrison, F., et al. (2006). Czt imaging detectors for protoexist. In *Hard X-Ray and Gamma-Ray Detector Physics and Penetrating Radiation Systems VIII*, volume 6319, page 63190S. International Society for Optics and Photonics.

Hubbell, J. H. and Seltzer, S. M. (1995). Tables of x-ray mass attenuation coefficients and mass energy-absorption coefficients 1 kev to 20 mev for elements z= 1 to 92 and 48 additional substances of dosimetric interest. Technical report, National Inst. of Standards and Technology-PL, Gaithersburg, MD (United ....

Kilerci-Eser, E., Goto, T., Guver, T., Tuncer, A., and Atas, O. H. (2020). Infrared colours and spectral energy distributions of hard x-ray selected obscured and compton-thick agn. *arXiv preprint arXiv:2004.01273*.

Koglin, J. E., Christensen, F. E., Craig, W. W., Decker, T. R., Hailey, C. J., Harrison, F. A., Hawthorn, C., Jensen, C. P., Madsen, K. K., Stern, M., Tajiri, G., and Taylor, M. D. (2005). NuSTAR hard x-ray optics. In Citterio, O. and O'Dell, S. L., editors, *Optics for EUV, X-Ray, and Gamma-Ray Astronomy II*, volume 5900, pages 266 – 275. International Society for Optics and Photonics, SPIE.

Koss, M. J., Assef, R., Baloković, M., Stern, D., Gandhi, P., Lamperti, I., Alexander, D. M., Ballantyne, D. R., Bauer, F. E., Berney, S., Brand t, W. N., Comastri, A., Gehrels, N., Harrison, F. A., Lansbury, G., Markwardt, C., Ricci, C., Rivers, E., Schawinski, K., Trakhtenbrot, B., Treister, E., and Urry, C. M. (2016). A New Population of Compton-thick AGNs Identified Using the Spectral Curvature above 10 keV. , 825(2):85.

Krivonos, R., Tsygankov, S., Lutovinov, A., Revnivtsev, M., Churazov, E., and Sunyaev, R. (2012). Integral/ibis nine-year galactic hard x-ray survey. *Astronomy & Astrophysics*, 545:A27.

Krivonos, R., Revnivtsev, M., Lutovinov, A., Sazonov, S., Churazov, E., and Sunyaev, R. (2007). Integral/ibis all-sky survey in hard x-rays ***. *A&A*, 475(2):775–784.

Lanzuisi, G., Ranalli, P., Georgantopoulos, I., Georgakakis, A., Delvecchio, I., Akylas, T., Berta, S., Bongiorno, A., Brusa, M., Cappelluti, N., Civano, F., Comastri, A., Gilli, R., Gruppioni, C., Hasinger, G., Iwasawa, K., Koekemoer, A., Lusso, E., Marchesi, S., Mainieri, V., Merloni, A., Mignoli, M., Piconcelli, E., Pozzi, F., Rosario, D. J., Salvato, M., Silverman, J., Trakhtenbrot, B., Vignali, C., and Zamorani, G. (2015). Compton thick agn in the xmm-cosmos survey. *A&A*, 573:A137.

Lebrun, F. (2006). The isgri cdte gamma camera in-flight performance. *Nuclear Science, IEEE Transactions on*, 52:3119 – 3123.

Liu, Y. and Li, X. (2014). An x-ray spectral model for clumpy tori in active galactic nuclei. *The Astrophysical Journal*, 787(1):52.

Malizia, A., Bassani, L., Bazzano, A., Bird, A., Masetti, N., Panessa, F., Stephen, J., and Ubertini, P. (2012). The integral/ibis agn catalogue—i. x-ray absorption properties versus optical classification. *Monthly Notices of the Royal Astronomical Society*, 426(3):1750–1766.

Malizia, A., Bassani, L., Bazzano, A., Bird, A. J., Masetti, N., Panessa, F., Stephen, J. B., and Ubertini, P. (2012). The INTEGRAL/IBIS AGN catalogue - I. X-ray absorption properties versus optical classification. , 426(3):1750–1766.

Malm, H. L. and Martini, M. (1974). Polarization phenomena in cdte nuclear radiation detectors. *IEEE Transactions on Nuclear Science*, 21(1):322–330.

Mateos, S., Warwick, R. S., Carrera, F. J., Stewart, G. C., Ebrero, J., Della Ceca, R., Caccianiga, A., Gilli, R., Page, M. J., Treister, E., Tedds, J. A., Watson, M. G., Lamer, G., Saxton, R. D., Brunner, H., and Page, C. G. (2008). High precision x-ray log n - log s distributions: implications for the obscured agn population*. *A&A*, 492(1):51–69.

Matt, G., Guainazzi, M., Frontera, F., Bassani, L., Brandt, W. N., Fabian, A. C., Fiore, F., Haardt, F., Iwasawa, K., Maiolino, R., Malaguti, G., Marconi, A., Matteuzzi, A., Molendi, S., Perola, G. C., Piraino, S., and Piro, L. (1997). Hard x–ray detection of ngc 1068 with bepposax.

Oh, K., Koss, M., Markwardt, C. B., Schawinski, K., Baumgartner, W. H., Barthelmy, S. D., Cenko, S. B., Gehrels, N., Mushotzky, R., Petulante, A., et al. (2018). The 105-month swift-bat all-sky hard x-ray survey. *The Astrophysical Journal Supplement Series*, 235(1):4.

Paczynski, B. (1971). Evolutionary processes in close binary systems. *Annual Review of Astronomy and Astrophysics*, 9(1):183–208.

Peterson, B. M. (1997). *An Introduction to Active Galactic Nuclei*. Cambridge University Press.

Photonics, H. (2000). *Photomultiplier tubes*. Hamamatsu.

Puccetti, S., Comastri, A., Fiore, F., Arévalo, P., Risaliti, G., Bauer, F. E., Brandt, W. N., Stern, D., Harrison, F. A., Alexander, D. M., Boggs, S. E., Christensen, F. E., Craig, W. W., Gandhi, P., Hailey, C. J., Koss, M. J., Lansbury, G. B., Luo, B., Madejski, G. M., Matt, G., Walton, D. J., and Zhang, W. (2014). THE VARIABLE HARD x-RAY EMISSION OF NGC 4945 AS OBSERVED BYNUSTAR. *The Astrophysical Journal*, 793(1):26.

Ramos Almeida, C. (2011). Testing the unification model for agn in the infrared: are the obscuring tori of type 1 and 2 seyferts different? In *IAC Talks, Astronomy and Astrophysics Seminars from the Instituto de Astrofísica de Canarias*.

Rosati, P., Tozzi, P., Giacconi, R., Gilli, R., Hasinger, G., Kewley, L., Mainieri, V., Nonino, M., Norman, C., Szokoly, G., Wang, J. X., Zirm, A., Bergeron, J., Borgani, S., Gilmozzi, R., Grogin, N., Koekemoer, A., Schreier, E., and Zheng, W. (2002). The Chandra Deep Field-South: The 1 Million Second Exposure. , 566(2):667–674.

Scaringi, S., Bird, A., Hill, A., Clark, D., McBride, V., Dean, A., Bazzano, A., Natalucci, L., and Stephen, J. (2010). A new determination of the integral/ibis point source location accuracy. *Astronomy & Astrophysics*, 516:A75.

Skinner, G. K. (2008). Sensitivity of coded mask telescopes. , 47(15):2739–2749.

Stern, D., Assef, R. J., Benford, D. J., Blain, A., Cutri, R., Dey, A., Eisenhardt, P., Griffith, R. L., Jarrett, T., Lake, S., et al. (2012). Mid-infrared selection of active galactic nuclei with the wide-field infrared survey explorer. i. characterizing wise-selected active galactic nuclei in cosmos. *The Astrophysical Journal*, 753(1):30.

Symeonidis, M., Giblin, B., Page, M., Pearson, C., Bendo, G., Seymour, N., and Oliver, S. (2016). Agn are cooler than you think: the intrinsic far-ir emission from qsos. *Monthly Notices of the Royal Astronomical Society*, 459(1):257–276.

Treister, E., Urry, C. M., and Virani, S. (2009). The Space Density of Compton-Thick Active Galactic Nucleus and the X-Ray Background. , 696(1):110–120.

Tsunemi, H., Hayashida, K., Tsuru, T. G., Dotani, T., Nakajima, H., Anabuki, N., Nagino, R., Tanaka, T., Uchida, H., Ozaki, M., et al. (2016). Soft x-ray imager (sxi) onboard astro-h. In *Space Telescopes and Instrumentation 2016: Ultraviolet to Gamma Ray*, volume 9905, page 990510. International Society for Optics and Photonics.

Türler, M., Chernyakova, M., Courvoisier, T. J. L., Lubiński, P., Neronov, A., Produit, N., and Walter, R. (2010). INTEGRAL hard X-ray spectra of the cosmic X-ray background and Galactic ridge emission. , 512:A49.

Ueda, Y., Akiyama, M., Hasinger, G., Miyaji, T., and Watson, M. G. (2014). Cosmological Evolution of X-ray Selected AGNs and Synthesis of the X-ray Background. In Mickaelian, A. M. and Sanders, D. B., editors, *Multiwavelength AGN Surveys and Studies*, volume 304 of *IAU Symposium*, pages 125–131.

Ueda, Y., Akiyama, M., Ohta, K., and Miyaji, T. (2003). Cosmological Evolution of the Hard X-Ray Active Galactic Nucleus Luminosity Function and the Origin of the Hard X-Ray Background. , 598(2):886–908.

Vasudevan, R., Brandt, W. N., Mushotzky, R., Winter, L. M., Baumgartner, W. H., Shimizu, T., Nousek, J. A., Schneider, D. P., and Gandhi, P. (2013). The Northern Galactic Cap AGN from the 58-month BAT Catalogue: A Comprehensive X-ray Spectral Study. In *AAS/High Energy Astrophysics Division #13*, AAS/High Energy Astrophysics Division, page 109.06.

Xue, Y. Q., Luo, B., Brandt, W. N., Bauer, F. E., Lehmer, B. D., Broos, P. S., Schneider, D. P., Alexand er, D. M., Brusa, M., Comastri, A., Fabian, A. C., Gilli, R., Hasinger, G., Hornschemeier, A. E., Koekemoer, A., Liu, T., Mainieri, V., Paolillo, M., Rafferty, D. A., Rosati, P., Shemmer, O., Silverman, J. D., Smail, I., Tozzi, P., and Vignali, C. (2011). VizieR Online Data Catalog: The CDF-S survey: 4Ms source catalogs (Xue+, 2011). *VizieR Online Data Catalog*, page J/ApJS/195/10.